Stark broadening of Kr III UV spectral lines

M. Ćirišan,[1] R. J. Peláez,[2] S. Djurović,[1] J. A. Aparicio,[2] and S. Mar[2]

[1]*Faculty of Sciences, Department of Physics, Trg Dositeja Obradovića 4, 21000 Novi Sad, Serbia*

[2]*Departamento de Física Teórica Atómica y Óptica, Facultad de Ciencias, Universidad de Valladolid, E-47011 Valladolid, Spain*

(Received 10 September 2010; published 24 January 2011)

This work reports new data for the Stark parameters of doubly ionized krypton spectral lines. Stark widths and shifts of Kr III lines belonging to the UV region (245–300 nm) have been measured. A low-pressure pulsed arc, containing a mixture of 8% krypton and 92% helium, was used as a plasma source. Measured electron densities and electron temperatures were in the range $(0.7–2.0)\times10^{23}$ m^{-3} and 16 000–20 000 K, respectively. Experimentally obtained data were compared to theoretical results calculated using simplified modified semiempirical formulas.

DOI: 10.1103/PhysRevA.83.012513 PACS number(s): 32.70.Jz, 32.30.Jc, 32.60.+i

I. INTRODUCTION

Stark broadening data of non-hydrogen spectral lines are of interest for studying both laboratory and astrophysical plasmas. Investigation of the ionized krypton spectra is significant for many reasons. First, spectra of inert gases are frequently analyzed in areas like laser physics, fusion diagnostics, photoelectron spectroscopy, collision physics, astrophysics, etc. Krypton plays an important role in industrial applications, like the development of spectral lamps [1], lasers, and laser techniques [2]. Furthermore, spectroscopic and atomic data of krypton ions are frequently employed for plasma diagnostic purposes, as well as for testing theoretical calculations. In addition, data on the Stark parameters of Kr III lines can be useful for investigating regularities and systematic trends of these parameters [3,4] among doubly ionized noble gases.

Although the interest exists, only a small number of experimentally determined Stark parameters data for Kr III UV lines can be found in the literature [5–9]. Only two publications report data on the Kr III Stark shift [8,9].

In this article we present measured data for the Stark parameters for 30 Kr III spectral lines. All data that belong to the wavelength region 245–300 nm are reported here. Stark halfwidths (full width at half maximum—FWHM) and shifts of spectral lines from $4d-5p$, $5s-5p$, $5d-5p$, and $5p-6s$ transition arrays have been measured. The results obtained have been compared to the halfwidths and shifts calculated using simplified modified semiempirical formulas [6].

The measurements were performed in a low-pressure pulsed arc plasma under the following conditions: electron density $(0.7–2.0)\times10^{23}$ m^{-3} and electron temperature 16 000–20 000 K. In this work, special attention was paid to both experimental and data treatment procedures. Other broadening mechanisms have also been taken into account.

With these results, we extend the current database of Stark parameters for the Kr III spectral lines to the UV region below 300 nm.

II. EXPERIMENT AND PLASMA DIAGNOSTICS

The measurements were performed under the same conditions as in our previous work, where Stark parameters of Kr II spectral lines have been determined [10]. The experimental apparatus and procedure has been described in detail in our previous works [11–13]. Here, only a few details will be given. The plasma was produced in a cylindrical tube of Pyrex glass, 175 mm in length and 19 mm in internal diameter. The gas mixture (8% Kr and 92% He) at a pressure of 2.6 kPa flowed continuously through the discharge tube. The gas in the tube was preionized by a continuous current of several mA in order to ensure plasma reproducibility. Plasma was created by discharging a capacitor bank of 20 μF charged up to 8200 V.

Spectroscopic measurements were performed along the discharge tube at a 2-mm distance from the tube axis. Light emitted from the plasma was limited by two diaphragms and focused by a concave mirror with a 150-mm focal length onto the entrance slit of a monochromator equipped with a 2400 lines/mm grating. The slit width of 35 μm was selected in order to obtain the best compromise between the intensity and the resolution. The spectrometer was calibrated in wavelength and spectral intensity with uncertainties less than 1% and 5%, respectively. The inverse linear dispersion at 300 nm was 3.5 pm/channel. Spectra were recorded by an intensified charge coupled device (ICCD) camera at 12 different instants of the plasma life, from 30 to 150 μs after the beginning of the discharge. The exposure time was usually 5 μs.

In order to minimize the effect of sputtering on the optical transmittance of the system, tube windows were replaced after every ~900 discharges, and the electrodes were polished several times during the experiment.

To determine the electron density, two-laser interferometry (wavelengths 543.0 and 632.8 nm) was used. The discharge tube was placed in one arm of a Twyman-Green interferometer. The laser beams, used for interferometric measurements [12], were directed along the discharge tube 2 mm off the tube axis symmetrically with respect to the direction of spectroscopic observations. This method is based on the fact that a variation of the plasma refractive index depends on the densities of the plasma species. By using two-wavelength interferometry, the influence of heavy particles on variations in the plasma refractive index is eliminated. Interferometric end-on measurements were performed during the plasma life, simultaneously with the spectroscopic measurements. Interferograms of 500 μs were recorded for each wavelength operating in the interferometer at every observed instant of the plasma life. Measured electron densities used for analyses in this work were in the range $(0.7–2.0)\times10^{23}$ m^{-3}. The error of electron density measurements was estimated to be lower than 10%. The intensities of 12 Kr II lines in the spectral interval

of 450 to 520 nm and their transition probabilities [14,15] have been used to obtain the excitation temperature by the Boltzmann-plot technique. In the temporal interval of interest in this experiment, the temperature was varied from 16 000 to 20 000 K. Statistical uncertainties for this plasma parameter were estimated to be lower than 15%.

III. EXPERIMENTAL DATA TREATMENT

Apart from taking care of experimental conditions and plasma diagnostics, attention was also paid to proper treatment of the experimental data. For each observation of the plasma life, ten spectra of the analyzed spectral interval were recorded; five with and five without a mirror placed behind the discharge tube, and the results of both recordings were averaged. The comparison of these two averaged spectra was used to check the self-absorption. The chosen percentage of krypton in the krypton-helium mixture ensured that, under these plasma conditions, self-absorption was absent for all spectral lines analyzed.

An incandescent calibrated lamp, emitting like a blackbody at 3041 K, and a deuterium lamp were used in order to obtain the spectrometer transmittance for all wavelengths of interest and for all ICCD channels. All spectra were corrected to this transmittance curve, whose uncertainty was estimated to be lower than 4%.

After this correction, the spectra were fit to a sum of asymmetrical Lorentzian functions representing spectral line profiles and a linear function representing the continuum [11]. For Kr III lines, asymmetry was negligible. This procedure allows one to measure the line intensity, center position, and line halfwidth, even in the case of overlapping spectral lines. The uncertainty of the line-wavelength determination was taken into account in the final experimental error.

The next step was the deconvolution procedure. Under these experimental conditions, Stark broadening was the dominant broadening mechanism. Two other pressure-broadening mechanisms (i.e., resonance and van der Waals broadening) were found to be negligible. Therefore, only Gaussian-(instrumental + Doppler) and Stark-broadening mechanisms were taken into account in this procedure [13,16].

IV. RESULTS AND DISCUSSION

Measured Stark parameters of 30 Kr III spectral lines are given in Table I. In the first three columns, Table I contains configurations, terms, and wavelengths of the observed spectral lines. In the next two columns, measured halfwidths w_m with estimated accuracy Acc and measured halfwidths expressed in angular frequency units w_ω, are presented. The sixth column contains the ratio between measured and calculated halfwidths, w_m/w_{SMSE}. The theoretical results were obtained from the simplified modified semiempirical halfwidth formula (SMSE) [6]. The last three columns contain measured Stark shifts d_m,with estimated accuracy Acc, measured shifts expressed in angular frequency units d_ω, and the ratio between measured and calculated shifts d_m/d_{SMSE}. The theoretical results were obtained from the simplified modified semiempirical shift formula [6]. All data are normalized to electron density $N_e = 1 \times 10^{23}$ m^{-3} and electron temperature $T_e = 18\,000$ K.

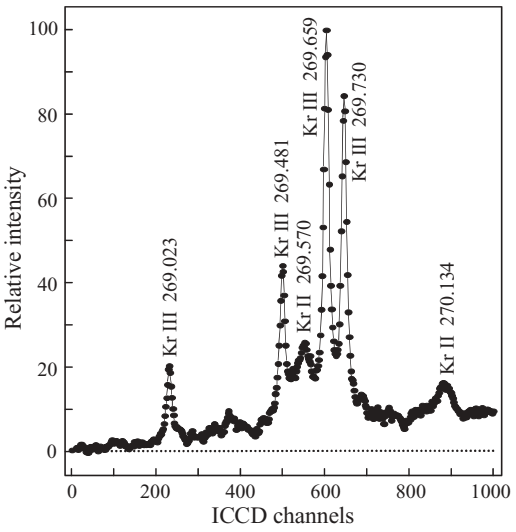

FIG. 1. Part of ionized krypton spectrum with close overlapping lines.

The multiplets are arranged in the same way as in the NIST atomic spectra database [17]. For multiplets number 10, 14–16, 18, 19, 21, and 26, two configurations and two-term symbols are given. Lower symbols correspond to data taken from the Striganov and Sventitskii tables [18].

A. Stark halfwidths

All measured Stark halfwidths show a linear dependence on electron density. As can be seen from Table I, under the plasma conditions in this experiment, Kr III spectral lines are very narrow (i.e., their halfwidths are between 10 and 30 pm). This is the reason why only spectral-line profiles corresponding to times between 30 and 65 μs have been considered in order to obtain the halfwidth values given in Table I. At those times, the electron density reaches its highest values, and the Stark broadening is maximal for our experimental conditions. This allows us to minimize the error in the deconvolution procedure. Furthermore, all possible errors in the line-shape recording, transmittance correction, as well as fitting and deconvolution procedure, were included in the final estimation of the experimental accuracy. Additional uncertainty is present in cases when several close spectral lines overlap, as shown in Fig. 1. In other cases, relatively large experimental errors are a consequence of a low signal-to-noise ratio, since we deal with low-intensity spectral lines. Depending on error estimation, the measured data presented in Table I are classified as A for errors up to 15%, B for errors up to 30%, and C for errors up to 50%. Classification was done in the same way as in the critical review paper [19] and later critical review papers by the same authors and their coauthors.

Within the observed spectral region, only the first multiplet in Table I contains a sufficient number of lines to analyze the intramultiplet halfwidth regularity. Within this multiplet, Stark halfwidth variation is less than $\pm 10\%$. According to [3], the variation of Stark halfwidths within a multiplet should be within several percent. Taking into account the estimated experimental errors, the Stark halfwidth regularity may be

TABLE I. Experimental Stark halfwidths w_m and shifts d_m of some Kr III UV lines normalized to electron density $N_e = 1 \times 10^{23}$ m^{-3} and electron temperature $T_e = 18\,000$ K. Estimated accuracy Acc: A ($< \pm 15\%$), B ($< \pm 30\%$), and C ($< \pm 50\%$) is given for both Stark parameters. Experimental results are compared to theoretical data calculated from the simplified modified semiempirical formula for halfwidths and formula for shifts (SMSE) [6]. There is only a limited number of other experimental results for the wavelength region considered; those from [8] are marked with * and those from [5] are marked with **.

No.	Configuration	Terms	Wavelength (nm)	w_m Acc (pm)	w_ω (10^{11} s^{-1})	w_m/w_{SMSE}	d_m Acc (pm)	d_ω (10^{10} s^{-1})	d_m/d_{SMSE}
1	$4s^24p^3(^4\mathrm{S}^\circ)4d - 4s^24p^3(^4\mathrm{S}^\circ)5p$	$^5\mathrm{D}_3{}^\circ - {}^5\mathrm{P}_3$	262.890	10.98 B	2.99	1.97	$\lvert d\rvert < 2$		
2		$^5\mathrm{D}_4{}^\circ - {}^5\mathrm{P}_3$	263.976	13.22 B	3.57	2.35	$\lvert d\rvert < 2$		
3		$^5\mathrm{D}_1{}^\circ - {}^5\mathrm{P}_2$	267.962	11.15 C	2.93	1.96			
4		$^5\mathrm{D}_2{}^\circ - {}^5\mathrm{P}_2$	268.032	13.38 B	3.51	2.35	$d < 2$		
5		$^5\mathrm{D}_3{}^\circ - {}^5\mathrm{P}_2$	268.119	12.79 B	3.35	2.25	$d < 2$		
6		$^5\mathrm{D}_0{}^\circ - {}^5\mathrm{P}_1$	269.481	12.22 B	3.17	2.15	2.03 B	−5.27	1.09
7		$^5\mathrm{D}_1{}^\circ - {}^5\mathrm{P}_1$	269.659	11.63 B	3.01	2.03	$d < 2$		
8		$^5\mathrm{D}_2{}^\circ - {}^5\mathrm{P}_1$	269.730	11.93 B	3.08	2.08	$d < 2$		
9	$4s^24p^3(^4\mathrm{S}^\circ)5s - 4s^24p^3(^4\mathrm{S}^\circ)5p$	$^3\mathrm{S}_1{}^\circ - {}^3\mathrm{P}_2$	350.742	21.46 A	3.29	0.95	$-2 < d < 0$		
						1.06 MSE			
				*19.32			*1.18		
10	$4s^24p^3(^2\mathrm{D}^\circ)4d - 4s^24p^3(^2\mathrm{D}^\circ)5p$	$^3\mathrm{F}_4{}^\circ - {}^3\mathrm{D}_3$	253.757	11.12 B	3.25				
	$4d' - 5p'$	$^3\mathrm{F}_4{}^\circ - {}^1\mathrm{F}_3$							
11		$^3\mathrm{F}_3{}^\circ - {}^3\mathrm{D}_2$	255.316	10.67 B	3.08				
12		$^3\mathrm{F}_2{}^\circ - {}^3\mathrm{D}_1$	269.023	10.69 B	2.78		$d < 2$		
13		$^3\mathrm{F}_2{}^\circ - {}^3\mathrm{F}_2$	255.425	11.40 C	3.29	2.24	$d < 2$		
14		$^3\mathrm{F}_3{}^\circ - {}^3\mathrm{F}_3$	255.513	10.73 C	3.10	2.04	$d < 2$		
		$^3\mathrm{F}_3{}^\circ - {}^3\mathrm{D}_3$							
15		$^3\mathrm{F}_4{}^\circ - {}^1\mathrm{F}_3$	257.119	10.74 B	3.06				
		$^3\mathrm{F}_4{}^\circ - {}^3\mathrm{F}_3$							
16		$^3\mathrm{G}_3{}^\circ - {}^3\mathrm{D}_2$	295.256	13.78 B	2.98		$\lvert d\rvert < 2$		
		$^3\mathrm{G}_3{}^\circ - {}^3\mathrm{F}_2$							
17		$^3\mathrm{G}_5{}^\circ - {}^3\mathrm{F}_4$	289.218	13.54 B	3.05	1.85	2.82 A	−6.35	1.56
18		$^3\mathrm{G}_4{}^\circ - {}^3\mathrm{F}_3$	299.222	14.33 B	3.02	1.92	$\lvert d\rvert < 2$		
		$^3\mathrm{G}_4{}^\circ - {}^3\mathrm{D}_3$							
19		$^3\mathrm{G}_4{}^\circ - {}^1\mathrm{F}_3$	289.368	14.64 B	3.29				
		$^3\mathrm{G}_4{}^\circ - {}^3\mathrm{F}_3$							
20	$4s^24p^3(^2\mathrm{D}^\circ)5s - 4s^24p^3(^2\mathrm{D}^\circ)5p$	$^3\mathrm{D}_1{}^\circ - {}^3\mathrm{D}_1$	364.134	24.48 C	3.48		−5.25 B	7.46	
21	$5s'–5p'$	$^3\mathrm{D}_3{}^\circ - {}^3\mathrm{F}_3$	347.465	20.40 A	3.18	0.98	−4.14 A	6.46	0.93
		$^3\mathrm{D}_3{}^\circ - {}^3\mathrm{D}_3$							
						1.02 MSE			0.87 MSE
				**18.50					
22		$^3\mathrm{D}_1{}^\circ - {}^3\mathrm{P}_0$	281.448	16.38 C	3.90	1.14			
23		$^3\mathrm{D}_2{}^\circ - {}^3\mathrm{P}_2$	290.004	13.53 C	3.03	0.89			
24	$4s^24p^3(^2\mathrm{P}^\circ)4d - 4s^24p^3(^2\mathrm{D}^\circ)5p$	$^1\mathrm{D}_2{}^\circ - {}^3\mathrm{P}_1$	299.660	14.72 C	3.09				
25		$^1\mathrm{D}_2{}^\circ - {}^1\mathrm{D}_2$	267.067	11.23 B	2.97				
26	$4s^24p^3(^2\mathrm{P}^\circ)4d - 4s^24p^3(^2\mathrm{D}^\circ)5p$	$^3\mathrm{P}_1{}^\circ - {}^3\mathrm{S}_1$	280.607	11.60 C	2.78				
	$4d'–5p''$	$^3\mathrm{S}_1{}^\circ - {}^3\mathrm{S}_1$							
27	$4s^24p^3(^2\mathrm{P}^\circ)4d - 4s^24p^3(^2\mathrm{P}^\circ)5p$	$^3\mathrm{F}_4{}^\circ - {}^3\mathrm{D}_3$	287.061	13.63 C	3.12	1.88	3.04 B	−6.95	1.71
28	$4s^24p^3(^4\mathrm{S}^\circ)5p - 4s^24p^3(^4\mathrm{S}^\circ)6s$	$^5\mathrm{P}_3 - {}^5\mathrm{S}_2{}^\circ$	256.325	29.11 B	8.35	1.16			
29	$4s^24p^3(^4\mathrm{S}^\circ)5p - 4s^24p^3(^4\mathrm{S}^\circ)5d$	$^5\mathrm{P}_2 - {}^5\mathrm{D}_3{}^\circ$	245.229	25.08 A	7.86	1.84			
30	$5p - 5d$	$^5\mathrm{P}_2 - {}^3\mathrm{D}_3{}^\circ$	245.772	19.56 C	6.10				

considered as satisfied. In other cases, the Stark-halfwidth-regularity check may be done only for supermultiplets or transition arrays. It was found that the Stark halfwidths of the lines belonging to the same transition array may differ within $\pm 40\%$ [3]. Here, there is a variation of the Stark halfwidths of about $\pm 15\%$ around the average value in case of all three transition arrays ($4d - 5p$, $5s - 5p$, and $5p - 5d$). The analysis shows a regular behavior of the line halfwidths. For this analysis, halfwidths expressed in angular frequency units (fifth column in Table I) were used in order to avoid the influence of the wavelength.

The last line in Table I exists only in Striganov and Sventitskii tables [18].

As already pointed out, this work presents measured Stark-parameter data for Kr III spectral lines below 300 nm. However, there are three data (numbers 9, 20, and 21 in Table I) for the lines above 300 nm: 350.742, 364.134, and 347.465 nm. Since there were no available experimental Stark-parameter

data from other authors in the investigated wavelength region, the data of the two lines 350.742 and 347.465 nm, which are situated close to the investigated wavelength region, were used for the comparison. The results of other authors are marked by * and ** in Table I. The ratios $w_m/w_{[8]} = 1.11$ and $w_m/w_{[5]} = 1.10$ show good agreement between our results and other authors' halfwidth results. There are a few measured Stark-parameter data in [9], but reliable plasma diagnostics parameters were not provided, so comparison with those results is not possible. The Stark parameters of the 364.134-nm line are also new results. This line belongs to the same transition array ($5s-5p$) as the 347.465-nm line and shows a regular behavior [3]. These results show, in an indirect way, the quality of the present experimental results.

In order to compare the experimentally obtained Stark halfwidths to the theoretical results, it is convenient to use modified semiempirical (MSE) calculations [20]:

$$w_{\rm th} = N_e \frac{8\pi}{3}\frac{\hbar^2}{m^2}\left(\frac{2m}{\pi kT}\right)^{1/2}\frac{\pi}{\sqrt{3}}\left[R^2_{l_i,l_i+1}\,\tilde{g}\left(\frac{E}{\Delta E_{l_i,l_i+1}}\right) + R^2_{l_i,l_i-1}\,\tilde{g}\left(\frac{E}{\Delta E_{l_i,l_i-1}}\right) + R^2_{l_f,l_f+1}\,\tilde{g}\left(\frac{E}{\Delta E_{l_f,l_f+1}}\right) + R^2_{l_f,l_f-1}\,\tilde{g}\left(\frac{E}{\Delta E_{l_f,l_f-1}}\right) + \sum_{i'}\left(R^2_{ii'}\right)_{\Delta n\neq 0} \times g\left(\frac{3kTn_i^3}{4Z^2E_{\rm H}}\right) + \sum_{f'}\left(R^2_{ff'}\right)_{\Delta n\neq 0} g\left(\frac{3kTn_f^3}{4Z^2E_{\rm H}}\right)\right], \quad (1)$$

where $E = 3kT/2$ is the energy of the perturbing electron, $\Delta E_{ll'} = |E_l - E_{l'}|$ is the energy difference between the levels l and the corresponding perturbing levels l'. Two types of matrix elements are calculated as

$$R^2_{l,l'} \approx \left(\frac{3n^*}{2Z}\right)^2 \frac{\max(l,l')}{2l+1}[n^{*2} - \max^2(l,l')]\Phi^2,$$
$$\sum_{j'}\left(R^2_{jj'}\right)_{\Delta n\neq 0} \approx \left(\frac{3n^*_j}{2Z}\right)^2 \frac{1}{9}\left(n^{*2}_j + 3l^2_j + 3l_j + 11\right), \quad (2)$$

where $n^*_j = [Z^2E_{\rm H}/(E_I - E_j)]^{1/2}$ is the effective principal quantum number [21], $E_{\rm H}$ and E_I are the ionization energies for hydrogen and the observed ion, respectively, l_j is the orbital angular momentum quantum number of the upper or lower energy state of the observed transition, and Z is the charge number. Φ^2 is the calculated Bates and Damgaard factor [22], which can also be found tabulated in Oertel and Shomo [23]. $g(x)$ and $\tilde{g}(x)$ are the corresponding Gaunt factors. Comparing to the semiempirical calculations [24], transitions with $\Delta n = 0$ are separated in the modified semiempirical formula (1). A complete set of perturbing levels, necessary for MSE calculations, is available only for two of the analyzed spectral lines (number 9, 350.742 nm and number 21, 347.465 nm). These comparisons are noted as MSE in Table I. For this reason, the experimental results were compared to the theoretical results obtained from simplified modified semiempirical (SMSE) formulas, which do not include positions of the perturbing levels in the calculation [6]:

$$\omega(\text{Å}) = 2.2151\times 10^{-8}\left[\frac{\lambda^2(\text{cm})N_e(\text{cm}^{-3})}{T_e^{1/2}(K)}\right]\left(0.9 - \frac{1.1}{z}\right) \times \sum_{j=i,f}\left(\frac{3n^*_j}{2z}\right)^2\left(n^{*2}_j - l_j{}^2 - l_j - 1\right). \quad (3)$$

Comparisons of the experimental and calculated results are given in the sixth column of Table I. However, even in this case, some data are missing (multiplets numbers 10–12, 15, 16, 19, 20, 24–26, and 30). First, there is a restriction for using formula [6]. In order to use this formula, it is necessary that the nearest perturbing level E'_j is far from the observed transition level E_j. This is expressed by the condition $E/\Delta E'_{jj} \leqslant 2$, where $E = 3kT/2$ is the energy of the perturbing electron and $\Delta E'_{jj} = |E_j - E'_j|$. A very good agreement between the experimental results and the calculated results exists only for the lines belonging to the $5s-5p$ and $5p-6s$ transitions. Generally, $w_m/w_{\rm SMSE}$ ratios vary between 0.95 and 2.3. This is expected, since formula [6] gives only a rough estimate of the Stark halfwidths. Second, for lines number 24–26 (Table I), there is a problem with a purity of the lower transition levels. For example, the lower transition level of 299.660 nm (number 24) is given as $(^2\text{P}^\circ)4d^1\text{D}_2{}^\circ$ in the NIST transition table [17], whereas in the NIST energy-levels table [17] it is given as $(^2\text{P}^\circ)4d^1\text{D}_2{}^\circ 24\% + (^2\text{D}^\circ)5s^1\text{D}_2{}^\circ 33\%$. There are two different orbital quantum numbers of the two components of the energy level. Different orbital quantum numbers lead to different values of the calculated halfwidths. There is a similar situation for the other two lines (numbers 25 and 26). This is the reason why the comparisons of the experimental and theoretical results for the lines from these multiplets are left out.

B. Stark shifts

Stark shifts were obtained using the method described in [25]. First, it was assumed that there was no Stark shift for the electron density $N_e = 0$. Since the exact position of an observed spectral line at $N_e = 0$ is unknown, this value was obtained by extrapolating the linear fit of the line's center position versus electron density to zero electron density. Once this value was subtracted from the measured line's center positions, the resulting differences multiplied by the inverse linear dispersion of the spectroscopic system gave us the desired Stark shift values (in pm). An example of shift measurement for the 287.061-nm line is given in Fig. 2.

From Table I, one can see that only five explicit shift values are given. The accuracy estimation was done in the same way as in the case of halfwidths, and it is given together with the shift values in column 7. In twelve cases, estimations of shift values are given as $|d| < 2$ or $d < 2$ pm. The value of 2 pm was estimated to be the precision of the shift determination for Kr III lines. For other spectral lines, the shift values are left out. The scattering of the points did not allow us to determine the line shift. It is well known that Stark shift measurements are, in general, less accurate than Stark halfwidth measurements, especially in cases where the shifts are very low.

Stark shifts of the lines belonging to the same multiplet may vary within ±10%, while the shifts of the lines within

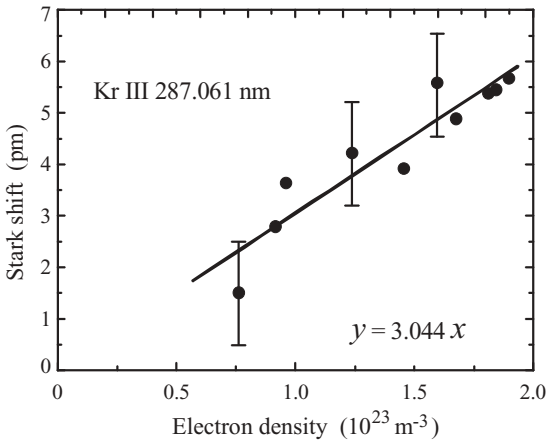

FIG. 2. Example of line shift versus electron density and its linear fit.

supermultiplets and transition arrays may differ within ±25% [4]. There are not enough explicit shift values to analyze the shift regularity within a multiplet (see Table I). The only thing we can say is that there is an agreement in shift direction within the multiplet ^{5}D – ^{5}P, if we exclude lines 262.890 and 263.976 nm from the analysis due to the uncertainty in their shift direction. For the supermultiplet-regularity analysis, there are only two shifts: lines 364.134 and 347.465 nm. The shifts of these lines vary by about ±7% around the average value. For the transition-array-regularity analysis, the explicit shift values exist only for three lines: 269.481, 289.218, and 287.061 nm. These lines belong to the $4d-5p$ transition array and vary around the average value for about ±15%. All shift values measured in this experiment, for which the analysis was possible, show a regular behavior according to [4]. For this analysis, shifts were expressed in angular frequency units (eighth column in Table I) in order to avoid the influence of the wavelength.

The experimental shift results were compared to theoretical data, in cases where it was possible. The measured shift of the 347.465-nm line (multiplet 21) is compared to the theoretical shift value calculated using the MSE formula [26]:

$$
\begin{aligned}
d = N\frac{h^2}{3\sqrt{3m}}\left(\frac{2m}{kT\pi}\right)^{\frac{1}{2}}\Bigg[& R^2_{l_i,l_i+1}\tilde{g}_{sh}\left(\frac{E}{\Delta E_{l_i,l_i+1}}\right) \\
& - R^2_{l_i,l_i-1}\,\tilde{g}_{sh}\left(\frac{E}{\Delta E_{l_i,l_i-1}}\right) - R^2_{l_f,l_f+1}\,\tilde{g}\left(\frac{E}{\Delta E_{l_f,l_f+1}}\right) \\
& + R^2_{l_f,l_f-1}\,\tilde{g}\left(\frac{E}{\Delta E_{l_f,l_f-1}}\right) + \sum_{i'}\left(R^2_{ii'}\right)_{\Delta n\neq 0} \\
& \times g_{sh}\left(\frac{E}{\Delta E_{n_i,n_i+1}}\right) - 2\sum_{i'(\Delta E_{ii'}<0)}\left(R^2_{ii'}\right)_{\Delta n\neq 0} g_{sh}\left(\frac{E}{\Delta E_{ii'}}\right) \\
& - \sum_{f'}\left(R^2_{ff'}\right)_{\Delta n\neq 0}\, g_{sh}\left(\frac{E}{\Delta E_{n_f,n_f+1}}\right) \\
& + 2\sum_{f'(\Delta E_{ff'}<0)}\left(R^2_{ff'}\right)_{\Delta n\neq 0} g_{sh}\left(\frac{E}{\Delta E_{ff'}}\right) + \sum_k \delta_k\Bigg], \qquad (4)
\end{aligned}
$$

where the sum $\sum_k \delta_k$ is nonzero only if $|\Delta E_{j'j}| \ll |\Delta E_{n,n+1}|$ [26].

The matrix elements are calculated in the same way as for halfwidth calculations (2). Formula (4) can be used under the same conditions as the MSE halfwidth formula (1).

In other cases, simplified modified semiempirical shift formula was used for the comparison [6]:

$$
\begin{aligned}
d(\text{Å}) \approx 1.1076\times 10^{-8}\frac{\lambda^2(\text{cm})N_e(\text{cm}^{-3})}{T_e^{1/2}(K)}\left(0.9-\frac{1.1}{z}\right) \\
\times\frac{9}{4Z^2}\sum_{j=i,f}\frac{\varepsilon n_j^{*2}}{2l_j+1}\left(n_j^{*2}-3l_j^2-3l_j-1\right), \qquad (5)
\end{aligned}
$$

where $\varepsilon = +1$ for $j = i$ and $\varepsilon = -1$ for $j = f$. The comparison results are given in the last column of Table I. All comments about SMSE shift calculations and necessary conditions for the calculations are the same as for halfwidths (3). The d_m/d_{SMSE} ratios vary between 0.93 and 1.71. This is expected for two reasons: formula [6] gives only a rough estimation of Stark shifts and, at the same time, Stark shift calculations are less accurate. The most important fact is that, independent of any discrepancy between measured and calculated shifts, direction of the shifts is the same in all cases (see Table I). There is only one disagreement in shift direction between the shift reported in [8] and the one measured and calculated here—for the 350.742-nm line; number 9 in Table I. Our shift estimation for this line is given as $-2 < d < 0$. The MSE and SMSE calculations also give a negative shift, while the shift reported in [8] is positive.

V. CONCLUSIONS

This work reports measured Stark halfwidths and data on Stark shifts of 30 doubly ionized krypton spectral lines from the UV region (245 to 300 nm). This is an extension of our work on Kr II Stark-parameter measurements [10]. Low-pressure arc plasmas were used for determination of the Stark parameters of the Kr III lines. Special attention was paid to experimental conditions, plasma diagnostics, as well as to treatment of the experimental data.

Presented results can extend the present database of measured Kr III Stark parameters to the UV region. There are experimental results from other authors devoted to Kr III UV lines, but only for the lines above 300 nm [5–9]. To make some connection with these results, we have extended our measurements to 360 nm. In that wavelength region, three well-defined spectral lines, 350.742, 364.134, and 347.465 nm, appear under our experimental conditions. Stark-parameter results for the 350.742-nm line are compared with the results from [8], while the Stark-halfwidth result of the 347.465-nm line is compared with the halfwidth result in [5]. Differences between the present results and the halfwidth results from [8] and [5] are less than 10%. This is an indirect way to confirm the validity of the present results.

Behavior of the Stark parameters was analyzed according to [3,4]. All measured Stark halfwidths show regular behavior. Differences between the halfwidths of the lines belonging to the multiplet ^{5}D – ^{5}P are less than ±10%, while the halfwidths within the supermultiplets and $4d-5p$ and $5s-5p$ transition

arrays vary about ±15% around the average halfwidth value. In case of Stark shifts, there are not enough explicit values to make a more general conclusion about their regularity. Experimental determination of line shifts is more sensitive to the signal-to-noise ratio, which is the reason why, in some cases, only the shift estimation is given.

The measured Stark parameters were compared to the theoretically calculated values. Measured Stark halfwidths and shifts were compared to the halfwidths and shifts calculated using the simplified modified semiempirical formula (SMSE) [6]. The w_m/w_{SMSE} ratio varies between 0.95 and 2.3, which is not so bad if one takes into account that the simplified modified semiempirical formula gives only a rough estimation of Stark halfwidths. Only a few halfwidths and shifts are compared to modified semiempirical calculations (MSE) [20,26]. A small number of shift data does not allow us to make any general conclusion. On the other hand, it is obvious that measured and calculated shift directions are in agreement if we exclude the cases with the uncertainty in shift direction. Detailed analysis about the agreement or disagreement between the experimental and calculated results is given in the text above. Present Stark-parameter data, in general, can be used for plasma diagnostic purposes, demonstration of regularities, and similarities of line halfwidths or shifts within the supermultiplets or transition arrays or, by combining them with other future experimental results, within the multiplets [3,4]. In addition, these results can be used for testing theory and applications and they can also be of interest in astrophysics.

ACKNOWLEDGMENTS

We thank S. González for his work on the experimental device, the Spanish Ministerio de Ciencia y Tecnología and the Consejería de Educación y Cultura de la Junta de Castilla y León for their financial support under contracts no. FIS2005–03155 and no. VA015A05, respectively. J. A. Aparicio wants to express his personal acknowledgment to the ONCE for help. S. Djurović thanks the Ministry of Science, Republic of Serbia for support in Project 171014.

[1] M. A. Cayless and A. M. Marsden, *Lamps and Lighting*, 3rd ed. (Edward Arnold, London, 1983).
[2] K. Shimoda, *Introduction to Laser Physics*, Springer Series in Optical Sciences, Vol. 44 (Springer, Berlin, 1984).
[3] W. L. Wiese and N. Konjević, J. Quant. Spectrosc. Radiat. Transfer **28**, 185 (1982).
[4] W. L. Wiese and N. Konjević, J. Quant. Spectrosc. Radiat. Transfer **47**, 185 (1992).
[5] N. Konjević and T. L. Pittman, J. Quant. Spectrosc. Radiat. Transfer **37**, 311 (1987).
[6] M. S. Dimitrijević and N. Konjević, Astron. Astrophys. **172**, 345 (1987).
[7] I. Ahmad, S. Büscher, Th. Wrubel, and H.-J. Kunze, Phys. Rev. E **58**, 6524 (1998).
[8] V. Milosavljević, S. Djenie, M. S. Dimitrijević, and L. Popović, Phys. Rev. E **62**, 4137 (2000).
[9] H. O. Di Rocco, G. Bertuccelli, J. Reyna Almandos, F. Bredice, and M. Gallardo, J. Quant. Spectrosc. Radiat. Transfer **41**, 161 (1989).
[10] S. Djurović, R. J. Peláez, M. Ćirišan, J. A. Aparicio, and S. Mar, Phys. Rev. A **78**, 042507 (2008).
[11] M. A. Gigosos, S. Mar, C. Pérez, and I. de la Rosa, Phys. Rev. E **49**, 1575 (1994).
[12] J. A. del Val, S. Mar, M. A. Gigosos, M. I. de la Rosa, C. Pérez, and V. R. González, Jpn. J. Appl. Phys. **37**, 4177 (1998).
[13] S. Djurović, R. J. Peláez, M. Ćirian, J. A. Aparicio, and S. Mar, J. Phys. B **39**, 2901 (2006).
[14] A. de Castro, J. A. Aparicio, J. A. del Val, V. R. González, and S. Mar, J. Phys. B **34**, 3275 (2001).
[15] S. Mar, J. A. del Val, F. Rodríguez, R. J. Peláez, V. R. González, A. B. Gonzalo, A. de Castro, and J. A. Aparicio, J. Phys. B **39**, 3709 (2006).
[16] R. J. Peláez, M. Ćirian, S. Djurović, J. A. Aparicio, and S. Mar, J. Phys. B **39**, 5013 (2006).
[17] NIST Atomic Spectra Database, [http://physics.nist.gov/asd3].
[18] A. R. Striganov and N. S. Sventitskii, *Tables of Spectral Lines of Neutral and Ionized Atoms* (Plenum, New York, 1968).
[19] N. Konjević and W. L. Wiese, J. Phys. Chem. Ref. Data **5**, 259 (1976).
[20] M. S. Dimitrijević and N. Konjević, J. Quant. Spectrosc. Radiat. Transfer **24**, 451 (1980).
[21] H. R. Griem, *Plasma Spectroscopy* (McGraw Hill, New York, 1964).
[22] R. D. Bates and A. Damgaard, Philos. Trans. R. Soc. London A **242**, 101 (1949).
[23] G. K. Oertel and L. P. Shomo, Astrophys. J. Suppl. Ser. **16**, 175 (1968).
[24] H. R. Griem, Phys. Rev. A **165**, 258 (1968).
[25] J. A. Aparicio, C. Pérez, J. A. del Val, M. A. Gigosos, M. I. de la Rosa, and S. Mar, J. Phys. B **31**, 4909 (1998).
[26] M. S. Dimitrijević and V. Krljanin, Astron. Astrophys. **165**, 269 (1986).